Analytical theory for the nonlinear optical response of a Kerr-type standing-wave cavity side-coupling to a MIM waveguide

Ye Liu,[1] Fei Zhou,[2] and Qinghe Mao[1,*]

[1] *Anhui provincial key lab of photonics devices and materials, Anhui Institute of Optics and Fine Mechanics, Chinese Academy of Sciences, Hefei, 230031, Anhui, China*

[2] *Key Laboratory of Materials Physics, Anhui Key lab of Nanomaterials and Nanotechnology, Institute of Solid State Physics, Chinese Academy of Sciences, Hefei, 230031, Anhui, China*

[*] *mqinghe@aiofm.ac.cn*

Abstract: In this article, an analytical theory to describe the nonlinear dynamic response characteristics of a typical SPP waveguide-cavity structure formed by a Kerr-type standing-wave cavity side-coupling to a metal-insulator-metal (MIM) waveguide is proposed by combining the temporal coupled mode theory and the Kerr nonlinearity. With the analytical theory, the optical bistability with the hysteresis behavior is successfully predicted, and the optical bistability evolutions and its dynamic physical mechanism are also phenomenologically analyzed. Moreover, the influence of the quality factors Q_0 and Q_1 on the first-turnning point (FTP) power of optical bistability and the bistable region width, the approaches to decrease the FTP power and to broaden the bistable region are also discussed in detail with our analytical theory. This work can help us understand the physical mechanism of the nonlinear dynamical response at nanoscale, and may be useful to design nonlinear nanophotonic systems for applications in ultra-compact all-optical devices and storages.

© 2013 Optical Society of America

OCIS codes: (240.6680) Surface plasmons; (190.1450) Bistability; (190.3270) Kerr effect.

References and links

1. W. L. Barnes, A. Dereux, and T. W. Ebbesen, "Surface plasmon subwavelength optics," Nature **424**, 824–830 (2003).
2. A. V. Zayats, I. I. Smolyaninov, and A. A. Maradudin, "Nano-optics of surface plasmon polaritons," Phys. Rep. **408**, 131–314 (2005).
3. J. Dionne, L. Sweatlock, H. Atwater, and A. Polman, "Plasmon slot waveguides: Towards chip-scale propagation with subwavelength scale localization," Phys. Rev. B **73**, 035407 (2006).
4. D. K. Gramotnev and S. I. Bozhevolnyi, "Plasmonic beyond the diffraction limit," Nat. Photonics **4**, 83–90 (2010).
5. D. Y. Fedyanin, A. V. Arsenin, V. G. Leiman, and A. D. Gladun, "Backward waves in planar insulator-metal-insulator waveguide structures," J. Opt. **12**, 015002 (2010).
6. T. Holmgaard and S. I. Bozhevolnyi, "Theoretical analysis of dielectric-loaded surface plasmon-polariton waveguides," Phys. Rev. B **75**, 245405 (2007).
7. G. X. Wang, H. Lu, and X. M. Liu, "Trapping of surface plasmon waves in graded grating waveguide system," Appl. Phys. Lett. **101**, 013111 (2012).
8. Q. Zhang, X. G. Huang, X. S. Lin, J. Tao, and X. P. Jin, "A subwavelength coupler-type MIM optical filter," Opt. Express **17**, 7549–7555 (2009).

#195038 - $15.00 USD Received 2 Aug 2013; revised 13 Sep 2013; accepted 13 Sep 2013; published 27 Sep 2013

9. Y. Hwang, J. Kim, and H. Y. Park, "Frequency selective metal-insulator-metal splitters for surface plasmons," Opt. Comm. **284**, 4778–4781 (2011).
10. A. Noual, A. Akjouj, Y. Pennec, J. N. Gillet, and B. D. Rouhani, "Modeling of two-dimensional nanoscale Y-bent plasmonic waveguides with cavities for demultiplexing of the telecommunication wavelengths," New J. Phys. **11**, 103020 (2009).
11. G. X. Wang, H. Lu, X. M. Liu, D. Mao, and L. N. Duan, "Tunable multi-channel wavelength demultiplexer based on MIM plasmonic nanodisk resonators at telecommunication regime," Opt. Express **19**, 3513–3518 (2011).
12. G. A. Wurtz and A. V. Zayats, "Nonlinear surface plasmon polaritonic crystals," Laser Photon. Rev. **2**, 125–135 (2008).
13. J. Tao, Q. J. Wang, and X. G. Huang, "All-optical plasmonic switches based on coupled nano-disk cavity structures containing nonlinear material," Plasmonics **6**, 753–759 (2011).
14. N. Nozhat and N. Granpayeh, "Switching power reduction in the ultra-compact Kerr nonlinear plasmonic directional coupler," Opt. Comm. **285**, 1555–1559 (2012).
15. H. Lu, X. M. Liu, L. R. Wang, Y. K. Gong, and D. Mao, "Ultrafast all-optical switching in nanoplasmonic waveguide with Kerr nonlinear resonator," Opt. Express **19**, 2910–2915 (2011).
16. K. F. MacDonald, Z. L. Samson, M. I. Stockman, and N. I. Zheludev, "Ultrafast active plasmonics," Nat. Photonics **3**, 55–58 (2009).
17. J. J. Chen, Z. Li, S. Yue, and Q. H. Gong, "Highly efficient all-optical control of surface-plasmon-polariton generation based on a compact asymmetric single slit," Nano Lett. **11**, 2933–2937 (2011).
18. J. X. Chen, P. Wang, X. L. Wang, Y. H. Lu, R. S. Zheng, H. Ming, and Q. W. Zhan, "Optical bistability enhanced by highly localized bulk plasmon polariton modes in subwavelength metal-nonlinear dielectric multilayer structure," Appl. Phys. Lett. **94**, 081117 (2009).
19. A. Pannipitiya, I. D. Rukhlenko, and M. Premaratne, "Analytical theory of optical bistability in plasmonic nanoresonators," J. Opt. Soc. Am. B **28**, 2820–2826 (2011).
20. X. S. Lin, J. H. Yan, Y. B. Zheng, L. J. Wu, and S. Lan, "Bistable switching in the lossy side-coupled plasmonic waveguide-cavity structrues," Opt. Express **19**, 9594–9599 (2009).
21. X. L. Wang, H. Q. Jiang, J. X. Chen, P. Wang, Y. H. Lu, and H. Ming, "Optical bistability effect in plasmonic racetrack resonator with high extinction ratio," Opt. Express **19**, 19415–19421 (2011).
22. H. Lu, X. M. Liu, Y. K. Gong, D. Mao, and L. R. Wang, "Enhancement of transmission efficiency of nanoplasmonic wavelength demultiplexer based on channel drop filters and reflection nanocavities," Opt. Express **19**, 12885–12890 (2011).
23. Y. Liu, F. Zhou, B. Yao, J. Cao, and Q. H. Mao, "High-extinction-ratio and low-insertion-loss plasmonic filter with coherent coupled nano-cavity array in a MIM waveguide," Plasmonics **8**, 1035–1041 (2013).
24. L. Liu, X. Hao, Y. T. Ye, J. X. Liu, Z. L. Chen, Y. C. Song, Y. Luo, J. Zhang, and L. Tan, "Systematical research on the characteristics of a vertical coupled Fabry-Perot plasmonic filter," Opt. Comm. **285**, 2558–2562 (2012).
25. J. D. Jackson, *Classical Electrodynamics* (John Wiley & Sons, Inc., 1999).
26. R. S. Irving, *Integers, Polynomials, and Rings* (Springer, 2004).
27. X. Y. Hu, P. Jiang, C. Y. Ding, H. Yang, and Q. H. Gong, "Systematical research on the characteristics of a vertical coupled Fabry-Perot plasmonic filter," Opt. Comm. **285**, 2558–2562 (2012).
28. Q. H. Mao and J. W. Y. Lit, "Optical bistability in an L-band dual-wavelength erbium-doped fiber laser with overlapping cavities," IEEE Photon. Technol. Lett. **14**, 1252–1254 (2002).
29. P. Berini and I. Leon, "Surface plasmon-polariton amplifiers and lasers," Nat. Photonics **6**, 16–23 (2012).

1. Introduction

Surface plasmon polaritons (SPPs) are electromagnetic modes coupled to the collective electron oscillations propagating along the interface between metallic and dielectric materials in visible or near-infrared optical frequency ranges [1, 2]. Previous research results have shown that plasmonic waveguides can confine the guided mode within the subwavelength-scale for overcoming the diffraction limit of light wave [3, 4]. To date, various SPP waveguide devices based on linear optics principles have been demonstrated [5–7]. Among them, the SPP devices with the resonant tunneling effect of nano-cavities have received more attention. With the single or multiple nano-cavity resonant coupling schemes, ultra-compact SPP filters, splitters, and WDM couplers have been proposed and designed [8–11]. In order to improve the flexibility in tuning and controlling for such SPP devices, recently nonlinear Kerr media have been introduced into the SPP waveguide-cavity coupling structures [12]. The performances of various SPP devices based on the Kerr nonlinearity have been investigated theoretically [13–15] and

#195038 - $15.00 USD Received 2 Aug 2013; revised 13 Sep 2013; accepted 13 Sep 2013; published 27 Sep 2013
(C) 2013 OSA

experimentally [16, 17]. Optical bistability, which is an important third-order optical nonlinear effect, has also been observed in different SPP waveguide-cavity structures [18, 19], and even used for the design of all-optical bistable SPP switches [20, 21]. However, almost all investigations of the optical bistability in SPP waveguide-cavity structure so far are based on numerical simulation methods, mainly the finite-difference time-domain (FDTD) technique, which makes it difficult to get insight to the fundamental physical mechanism of such an optical bistability phenomenon. In this article, by combining the temporal coupled mode theory (TCMT) and the Kerr nonlinearity, an analytical theory for describing the dynamic response characteristics of an SPP waveguide-cavity structure formed by a nonlinear standing-wave cavity side-coupling to a MIM waveguide is presented. The optical bistability and its dynamic physical process is predicted and discussed with the analytical theory.

2. Analytical theory

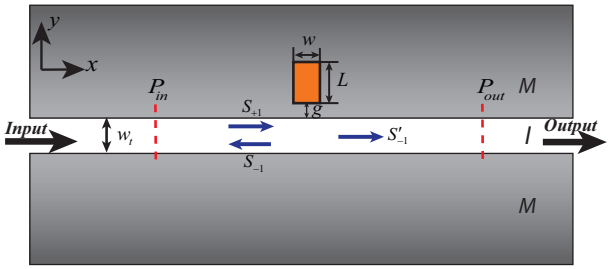

Fig. 1. Typical plasmonic structure with a Kerr nonlinear cavity side-coupling to a MIM waveguide.

Figure 1 shows a typical plasmonic structure with a Kerr nonlinear cavity side-coupling to a linear dielectric waveguide. The waveguide (white region) and the Kerr nonlinear cavity (orange region) are buried in a metal substrate (gray region). Assuming that both the cavity and the waveguide support only one mode in the frequency range of interest, thus, if the amplitudes of the incident, refractive, and transmitted lights in the waveguide are respectively denoted by S_{+1}, S_{-1} and S_{-1}', then, according to the TCMT, the time evolution for the amplitude of resonant cavity mode, A, may be described as [22, 23]

$$\frac{dA}{dt} = (j\omega_c - \frac{\omega_c}{Q_0} - \frac{\omega_c}{2Q_1})A + \sqrt{\frac{\omega_c}{2Q_1}}e^{j\theta}S_{+1}, \tag{1}$$

with

$$S_{-1}' = S_{+1} - \sqrt{\frac{\omega_c}{2Q_1}}e^{-j\theta}A$$

$$S_{-1} = -\sqrt{\frac{\omega_c}{2Q_1}}e^{-j\theta}A$$

where ω_c is the resonant frequency of the cavity, Q_0 is the quality factor due to the intrinsic cavity loss, Q_1 is the quality factor that is related to the decay rate into the waveguide, and θ stands for the phase change of the coupling between the guided SPP and the cavity resonator mode.

If S_{+1} has a time dependence of $e^{j\omega t}$, the steady-state transmission of the plasmonic structure

#195038 - $15.00 USD Received 2 Aug 2013; revised 13 Sep 2013; accepted 13 Sep 2013; published 27 Sep 2013
(C) 2013 OSA

can be expressed as

$$T = \left|\frac{S_{-1}{}'}{S_{+1}}\right|^2 = \frac{(\frac{\omega}{\omega_c}-1)^2 + (\frac{1}{Q_0})^2}{(\frac{\omega}{\omega_c}-1)^2 + (\frac{1}{Q_0}+\frac{1}{2Q_1})^2}. \tag{2}$$

And, the total energy in the cavity $|A|^2$ and the incident power $|S_{+1}|^2$ (or P_{in}) satisfies:

$$|A|^2 = \frac{\frac{1}{2\omega_c Q_1}}{(\frac{\omega}{\omega_c}-1)^2 + (\frac{1}{Q_0}+\frac{1}{2Q_1})^2}|S_{+1}|^2. \tag{3}$$

From Eq. (3) it can be clearly seen that the energy in the cavity increases with the incident power, which results in the changes of nonlinear refractive index. Strictly, the resonant frequency ω_c and the quality factors Q_0 and Q_1 may change with the nonlinear refractive index variation of the cavity. However, if only weak Kerr nonlinearity, i.e., the nonlinear refractive index $\Delta n < 5\%$, is considered, the tiny changes of Q_0 and Q_1 due to the Kerr nonlinearity can be ignored. Thus, in the TCMT treatment for the plasmonic structure shown in Fig. 1, only the variation of the resonant frequency caused by the Kerr nonlinearity may be taken into accounted.

On the other hand, an arbitrary standing-wave cavity side-coupling to a MIM waveguide may be regarded as a Fabry-Perot cavity [24, 25], whose resonant wavelength can be described as $2(n_{eff}L_{eff}+2L_{pen}) = N\lambda_c (N = 1,2,3,\cdots)$, with L_{pen}, n_{eff} and L_{eff} respectively being the penetration depths at two ends, the effective refractive index and the effective length of the F-P cavity. For the weak Kerr nonlinearity cavity with only single resonant mode, the resonant wavelength of the cavity can be written as:

$$\lambda_c = \lambda_{c0} + 2n_2\left\langle |E_b|^2 \right\rangle L_{eff} = \lambda_{c0} + \frac{2n_2 L_{eff}|A|^2}{\varepsilon S} \tag{4}$$

where λ_{c0} is the linear resonant wavelength, n_2 is the Kerr nonlinear-index coefficient, and $\langle |E_b|^2 \rangle = |A|^2/(\varepsilon S)$ is the average electric field intensity in the cavity with S and ε being the area and the permittivity of the cavity, respectively.

Substituting Eq. (3) into Eq. (4), using $\lambda_c = 2\pi c/\omega_c$ and $|S_{+1}|^2 = P_{in}$, we can get a cubic equation with λ_c after eliminating the term of $|A|^2$:

$$\lambda_c{}^3 + B\lambda_c{}^2 + (C_1 - C_2 P_{in})\lambda_c + D = 0, \tag{5}$$

where $B = -(2\lambda + \lambda_{c0})$, $C_1 = \lambda^2\left[1+(1/Q_0+1/(2Q_1))^2\right] + 2\lambda\lambda_{c0}$, $C_2 = n_2 L_{eff}\lambda^2/(2\pi c Q_1 \varepsilon S)$, and $D = -\lambda_{c0}\lambda^2\left[1+(1/Q_0+1/(2Q_1))^2\right]$. From Eq. (5), we can see that, for a given structure of the standing-wave cavity side-coupling to a MIM waveguide, λ_c exhibits strong nonlinear relationship with the wavelength λ and the power P_{in} of the incident light.

In order to further explore the nonlinear relationship of λ_c with λ and P_{in}, we may find the derivative of P_{in} with respect to λ_c from Eq. (5), and let $dP_{in}/d\lambda_c = 0$, then we have

$$\lambda_c{}^3 + \frac{B}{2}\lambda_c{}^2 - \frac{D}{2} = 0. \tag{6}$$

Note that B and D are just functions of the incident light wavelength λ for a given waveguide-cavity structure. In general, Eq. (6) may have three distinct real roots if its discriminant is less than zero, i.e., $\Delta < 0$. If assuming λ_{c1}, λ_{c2} and λ_{c3} are respectively the three distinct real roots of Eq. (6), then, they must spontaneously satisfy: (1) $\lambda_{c1}+\lambda_{c2}+\lambda_{c3} = -B/2$, which is constantly

#195038 - $15.00 USD Received 2 Aug 2013; revised 13 Sep 2013; accepted 13 Sep 2013; published 27 Sep 2013
(C) 2013 OSA

larger than zero, and (2) $\lambda_{c1}\lambda_{c2}\lambda_{c3} = D/2$, which is always less than zero. This indicates that there must be two positive and a negative real numbers among λ_{c1}, λ_{c2}, and λ_{c3} when $\Delta < 0$ for Eq. (6). In fact, the existence of the two positive real roots for Eq. (6) means that there are two knee points for the $P_{in} \sim \lambda_c$ curve, and thus, implies that there may exist some optical bistability phenomenon when λ is suitably chosen to ensure $\Delta < 0$.

To determine the range of λ for the optical bistability, according to the critical condition $\Delta = 0$, we have

$$x^3 - \frac{27\zeta^2 + 15}{8}x^2 + \frac{3}{4}x + \frac{1}{8} = 0 \tag{7}$$

where $x = \lambda/\lambda_{c0}$ and $\zeta = 1/Q_0 + 1/(2Q_1)$. We can then get the two positive real roots by solving Eq. (7) [26]

$$x_{1,2} = -\frac{B'}{3} + e^{\pm i\frac{2\pi}{3}}\sqrt[3]{-\frac{q'}{2} + \sqrt{\Delta'}} + e^{\mp i\frac{2\pi}{3}}\sqrt[3]{-\frac{q'}{2} - \sqrt{\Delta'}}$$

where $B' = (27\zeta^2 + 15)/8$, $q' = (27 - 459\zeta^2)/256$, and $\Delta' = -(27\zeta/64)^2$. Since ζ is in the order of 10^{-2}, the higher order terms of ζ may be ignorable. Then, we have

$$x_{1,2} = 1 \pm \sqrt{3}\zeta$$

or

$$\lambda - \lambda_{c0} = \pm\sqrt{3}\lambda_{c0}\left(\frac{1}{Q_0} + \frac{1}{2Q_1}\right) = \pm\frac{\sqrt{3}\Delta\lambda}{2} \tag{8}$$

where $\Delta\lambda = 2\lambda_{c0}\,(1/Q_0 + 1/(2Q_1))$ is the FWHM of the linear transmission spectrum, which can be easily obtained from Eq. (2).

Based on the discussion as the above, if the critical wavelength λ_M is defined as $\lambda_M = \lambda_{c0} + \sqrt{3}\Delta\lambda/2$ (or $\lambda_M = \lambda_{c0} - \sqrt{3}\Delta\lambda/2$) for the positive (or negative) nonlinearity, it can be found that, when $\lambda > \lambda_M$ (or $\lambda < \lambda_M$) , the discriminant of Eq. (6) is less than zero, and thus two different λ_c truly exist for a specific given P_{in}, leading to the occurrence of optical bistability phenomenon.

3. Results and discussions

Firstly, we consider a Kerr nonlinear cavity side-coupling to a MIM waveguide (see Fig. 1) with specifications of $Q_0 = 235$, $Q_1 = 65$, $\lambda_{c0} = 1556.9$ nm, $S = 3.6 \times 10^4$ nm^2, $L_{eff} = 360$ nm, and $n_2 = 1 \times 10^{-8}$ cm^2/W [27], respectively. These parameters correspond to a plasmonic structure of an Ag-SiO_2-Ag waveguide with a side-coupling nonlinear polystyrene rectangular cavity shown in Fig. 1, whose structure parameters are $w_t = 50$ nm, $w = 100$ nm, $L = 360$ nm, and $g = 15$ nm. According to our theory described in the above, when the incident light wavelength is larger than $\lambda_M = 1589.1$ nm, the optical bistability phenomenon may occur. To test the validity of our prediction, the transmission as a function of P_{in} is calculated for different given λ by using Eqs. (2) and (5), and the results are shown in Fig. 2(a). Note that the calculation results with our analytical model and the finite-difference time-domain (FDTD) technique [19] for 1610 nm are also given in Fig. 2(b), which shows they are in good agreement with respect to each other, indicating the validation of our analytical model. Figure 2(a) clearly shows that the optical bistability with the hysteresis behavior occurs only when λ is larger than 1589.1 nm. Otherwise, no bistability phenomenon is exhibited. However, when the incident wavelength is smaller than 1589.1 nm, the transmission can be continuously adjusted in a large range by only slightly changing the incident power near the transmission dip, such a property may be used to design all-optical switches.

#195038 - $15.00 USD Received 2 Aug 2013; revised 13 Sep 2013; accepted 13 Sep 2013; published 27 Sep 2013
(C) 2013 OSA

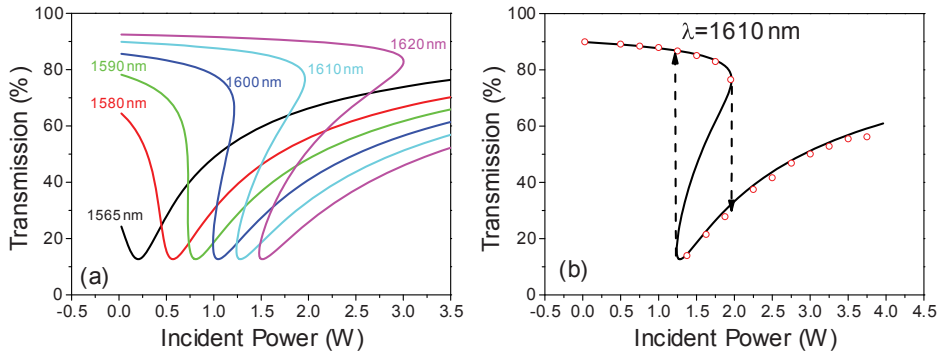

Fig. 2. (a) Transmissions as a function of incident power for different incident light wavelengths; (b) The comparisons of the bistable curves obtained by our analytical theory (solid line) and the FDTD numerical simulations (red circles).

The transmission variations shown in Fig. 2(a) may be explained with our analytical theory. According to Eq. (3), the energy coupled into the cavity is increased with the increasing of P_{in}. However, the increasing speed of the cavity energy with P_{in} depends on the incident light wavelength. When λ is less than λ_M, the difference between λ and λ_{c0} is small, making λ to be within the cavity resonance band in the beginning [see Fig. 3(a)]. Thus, even if the initial incident power is low, the proportion of the power coupled into the cavity is still high, which makes an obvious red-shift of λ_c. For instance, when the incident light wavelength is fixed at 1580 nm, as shown in Fig. 3(b), a red-shift about 5 nm for λ_c respect with to λ_{c0} has been made if the incident power is increased to 0.25 W from zero. This red-shift of λ_c can further strengthen the resonant coupling effect between the cavity and the waveguide, which in turn speeds up the red-shifted of λ_c to be close to λ [see Fig. 3(b)], forming a positive feedback mechanism. This positive feedback mechanism makes the transmissions decreases monotonously with the increase of P_{in} and reaches to their minimum rapidly at which $\lambda_c = \lambda$. Such a property of the transmissions decreasing monotonously to their minimum by slightly changing P_{in} may be used for the design of all-optical switches, as mentioned before. If then P_{in} is further increased, λ_c may be gradually larger than λ because of the red-shift effect caused by the Kerr nonlinearity. This results in the weakened resonant coupling between the cavity and the waveguide which retards the red-shifted λ_c to be away from λ, forming a negative feedback mechanism. This negative feedback mechanism can help λ to stay in the cavity resonance band with the center wavelength of λ_c, finally resulting that the transmissions increases slowly with the increase of P_{in} from their minimal values. As the incident power decreases from a high level, a reverse process is exhibited, and no hysteresis behavior occurs due to the monotonous changes of λ_c.

When λ is larger than λ_M, as shown in Fig. 3(a), λ is far away from the linear cavity resonance band near λ_{c0} in the beginning, and the proportion of the power coupled into the cavity is very low. This causes that the energy in the cavity increases very slowly with the increase of P_{in} from zero, and thus, the Kerr nonlinearity gives an ignorable red-shift for λ_c. For an example, when the incident wavelength is 1610 nm, as shown in Fig. 3(c), a 5 nm red-shift of λ_c cannot be obtained until the incident power is increased to 1.0 W. Such a red-shift of λ_c is not large enough to make λ_c being close to λ. Because of this reason, the transmissions for $\lambda > \lambda_M$ keep staying in high levels until P_{in} has been increased to high enough to trigger the positive feedback mechanism described in the above, which results that the transmissions jump down to the low branches shown in Fig. 2. This specific P_{in} is so-called the first turning point

#195038 - $15.00 USD Received 2 Aug 2013; revised 13 Sep 2013; accepted 13 Sep 2013; published 27 Sep 2013
(C) 2013 OSA

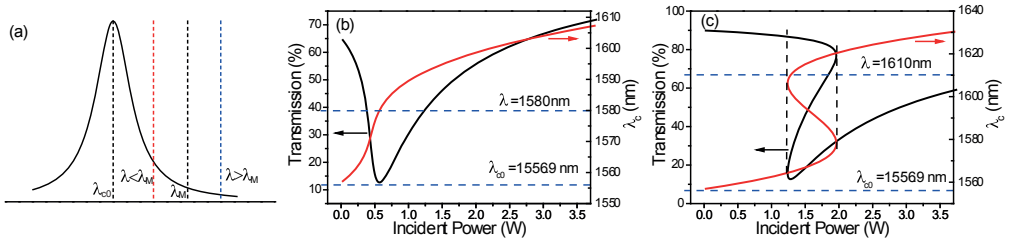

Fig. 3. (a) Schematic diagram for the linear transmission properties when the incident wavelength is larger or less than λ_M respectively; (b) and (c) Transmissions (black line) and nonlinear resonant wavelengths (red line) as a function of incident light power for the incident light wavelength of 1580 and 1610 nm, respectively. The linear resonant wavelength and the incident light wavelengths are displayed with blue dot lines in (b) and (c).

(FTP) power, where a sudden red-shift of λ_c takes place [28]. Note that λ_c is larger than λ once the transmission has jumped down to the low branch, just as shown in Fig. 3(c) in which λ_c jumps from 1578 nm to 1620 nm at the FTP for $\lambda = 1610$ nm. After then, like the case of $\lambda < \lambda_M$, the negative feedback mechanism also helps λ stay in the cavity resonance band near λ_c, and the transmission increases slowly with the increase of P_{in}. However, if P_{in} is decreased from a high level, since λ is located in the cavity resonance band near λ_c in the beginning, the resonant energy in the cavity can keep in a high level with the negative feedback mechanism even if P_{in} has been decreased to a level less than the FTP. This negative feedback mechanism can be maintained until $\lambda_c = \lambda$, where the minimal transmission is reached. If P_{in} decreases furtherly, λ_c will continue to blue-shift and a positive feedback happen. When P_{in} decreases to a level called as the second turning point (STP), the positive feedback mechanism will result in a sudden blue-shift of λ_c [from 1606 nm to 1564 nm in Fig. 3(c)] with a tiny increase of P_{in}, which makes the transmission jumps up to the up-branch. After this jump, the transmission is increased slowly again with the decrease of P_{in} due to the tiny blue-shift of λ_c. Finally the optical bistability with the hysteresis behavior occurs for the case of $\lambda > \lambda_M$.

Obviously, the cavity energy storage capability, determined by Q_0 and Q_1, may affect the above hysteresis bistability behavior. Figures 4(a) and 4(b) show the critical wavelength λ_M as a function of Q_0 and Q_1, respectively. As seen, for a given Q_1 of 65, λ_M decreases from 1605 nm to 1582 nm when Q_0 increases from 100 to 400. When Q_1 increases from 40 to 100, the same change for λ_M can be obtained for a given Q_0 of 235. The decrease of λ_M is originated from the less energy attenuation in the cavity with larger Q_0 or Q_1. Figure 4(c) shows the transmission at 1610 nm as a function of the incident power for different Q_0 when Q_1 is fixed at 65. Here, we can see that, with the increase of Q_0, i. e., the decrease of the intrinsic cavity loss, both the FTP and the STP powers are decreased, with STP being decreased more, making that the bistalbe regions become wider. When Q_0 increases from 100 to 400, the FTP and the STP powers reduce from 3 W to 2 W, and from 2.78 W to 0.9 W, respectively. The corresponding bistalbe region is increased from 0.22 W to 1.1 W. However, for a given Q_0, the FTP and the STP power may respectively be increased and decreased with the increase of Q_1 because the weakend coupling strength between the waveguide and the cavity causes the decreases of both the incoming and outcoming energies for the cavity, thus giving wider bistable regions. Figure 4(d) shows such situations. From this figure it can be seen that when Q_1 increases from 40 to 100, the FTP power increases from 1.6 W to 2.6 W, and the STP power reduces from 1.55 W to 1.25 W, resulting that the bistable region is broadened from 0.05 W to 1.35 W. Therefore, in order to reduce the FTP power of optical bistability, larger Q_0 and smaller Q_1 are preferred. Considering that the width of the bistable region may be narrowed by decreasing Q_1, an optimized way for reducing

#195038 - $15.00 USD Received 2 Aug 2013; revised 13 Sep 2013; accepted 13 Sep 2013; published 27 Sep 2013
(C) 2013 OSA

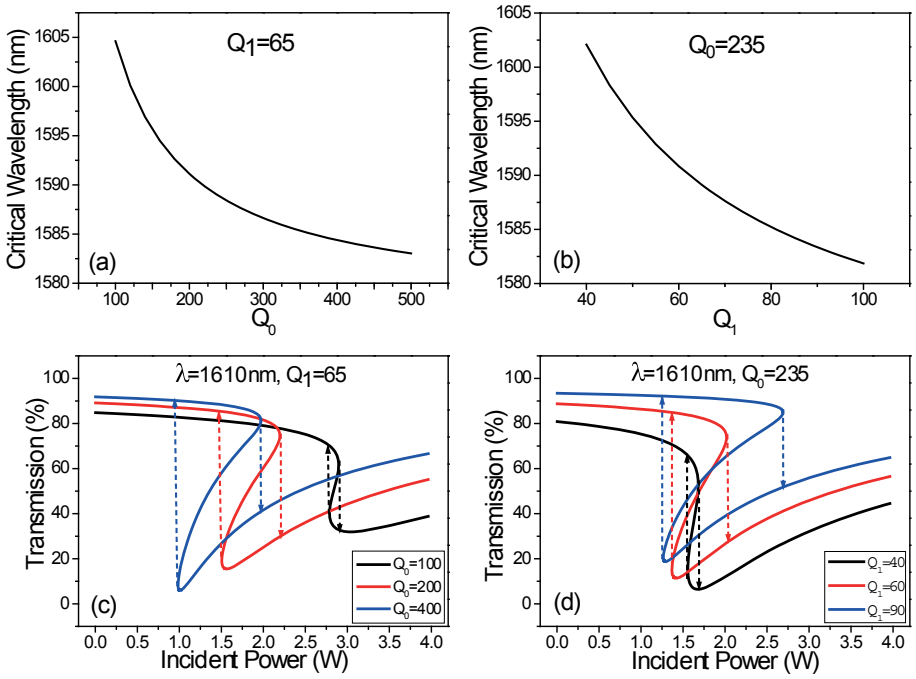

Fig. 4. The critical wavelength of optical bistability as a function of (a) Q_0 and (b) Q_1 for a fixed Q_1 and Q_0, respectively. Bistable properties at 1610 nm for (c) different Q_0 and (d) different Q_1 when Q_1 and Q_0 are fixed, respectively.

FTP power is to increase the value of Q_0 as much as possible, which may be achievable by using optical gain in the cavity to compensate its intrinsic loss [29].

4. Conclusions

By combining the TCMT and the Kerr nonlinearity, an analytical theory for describing the dynamic response characteristics of an SPP waveguide-cavity structure formed by a nonlinear standing-wave cavity side-coupling to a MIM waveguide has been presented. The criterion that $\lambda > \lambda_{c0} + \sqrt{3}\Delta\lambda/2$ ($n_2 > 0$) or $\lambda < \lambda_{c0} - \sqrt{3}\Delta\lambda/2$ ($n_2 < 0$) given in the analytical theory can be used to predict whether the optical bistability with the hysteresis behavior takes place. The optical bistability evolutions and its dynamic physical mechanism can also be phenomenologically analyzed with the analytical theory. Moreover, by using our analytical theory, the influence of Q_0 and Q_1 on the FTP power and the bistable region width is clarified, and the approaches to decrease the FTP power and to broaden the bistable region are also obtained. Our results may be helpful to get deep insight into the fundamental physics of the nonlinear dynamic response in nanoscale plasmonic waveguide devices and may be beneficial in their designs and optimizations.

Acknowledgments

This work is supported by the National Natural Science Foundation of China under Grant Nos. 11104282, 11204317 and 61250017, and by the National Basic Research Program of China under Grant No. 2011CB934304.

#195038 - $15.00 USD Received 2 Aug 2013; revised 13 Sep 2013; accepted 13 Sep 2013; published 27 Sep 2013
(C) 2013 OSA